ACS Catalysis

pubs.acs.org/acscatalysis

Research Article

Oxyl Character and Methane Hydroxylation Mechanism in Heterometallic $M(O)Co_3O_4$ Cubanes (M = Cr, Mn, Fe, Mo, Tc, Ru, and Rh)

Bastian Bjerkem Skjelstad, Trygve Helgaker, Satoshi Maeda, and David Balcells*

Cite This: *ACS Catal.* 2022, 12, 12326−12335

Read Online

ACCESS | Metrics & More | Article Recommendations | Supporting Information

ABSTRACT: C−H activation in alkanes poses a major challenge in chemistry due to the inert character of this bond, manifesting the necessity of improved catalysts. Although various metal−oxo complexes are known to facilitate alkane hydroxylation, probing the mechanistic nature of the reaction is difficult due to the extremely fast rebound of the radical intermediate in the postulated oxygen-rebound pathway. Automated reaction mechanism discovery methods, such as the artificial force induced reaction (AFIR) method, enable the efficient exploration of both expected and unexpected reaction pathways, revealing the reaction mechanism. Here, we employed this approach combined with density-functional theory (DFT) to investigate the structure and reactivity of heterometallic cubane complexes similar to the oxygen-evolving complex of photosystem II. For a series of $M(O)Co_3O_4$ cubanes, where $M(O)$ is a terminal oxo with M = Cr, Mn, Fe, Mo, Tc, Ru, and Rh, we computed the stability of the possible spin states and the radical (*i.e.*, oxyl) character of the $M(O)$ moiety as a measure of their potential activity in the catalytic hydroxylation of alkanes. DFT calculations on these reactions promoted by $Ru(O)Co_3O_4$ and $Fe(O)Co_3O_4$ suggest that the latter promotes the hydroxylation of methane with a rate-determining H-abstraction barrier of 24.6 kcal/mol. The moderate height of this barrier, together with the low cost and low toxicity of iron and cobalt, suggests that the $Fe(O)Co_3O_4$ cubane is a promising candidate for the catalytic oxidation of methane to methanol. AFIR calculations showed that the oxygen-rebound pathway yields the lowest-energy profile, thus validating this mechanism for the hydroxylation of alkanes by heterometallic cubanes. Furthermore, unexpected intermediates in which the methyl radical couples with either the metal center or the bridging oxo ligands were also observed.

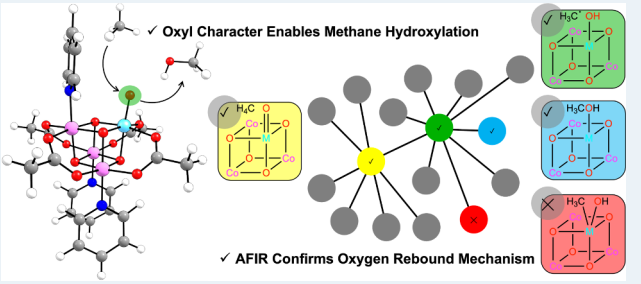

KEYWORDS: *methane, oxidation, mechanism, rebound, DFT, AFIR, iron*

INTRODUCTION

Multimetallic oxo cubanes are an intriguing class of transition metal (TM) complexes with significant potential as catalysts.[1] One example of such a structure found in nature is the oxygen-evolving complex (OEC) in photosystem II, containing a Mn_4CaO_5 cubane cluster[2,3] that oxidizes water to molecular oxygen in a stepwise fashion through the Kok cycle.[4−6] Inspired by nature, several cubane complexes that mimic the OEC have been synthesized, including the homometallic Mn_4O_4[7−9] and Co_4O_4[10−13] cubanes and the heterometallic $MnCo_3O_4$,[14] $Ru(O)Co_3O_4$,[15] and $MnCo_4O_4$[16] cubanes (Figure 1).

We have previously investigated the electronic properties and reactivity of several of these complexes, including the $[MnCo_3CoO_4(OAc)_6(NO_3)(py)_3]$,[16] $[Co_4O_4(OAc)_4(py)_4]$,[17] and $[Ru(O)Co_3O_4(OAc)_4(py)_3]$[15,18] cubanes (OAc = acetate, py = pyridine). Our investigations showed that these complexes have a remarkable potential for C−H activation catalysis due to the localization of the radical character on the oxygen (oxyl) abstracting the H atom from the alkane and due to a significant metal−metal cooperativity at the core of the cubic oxide. In particular, the terminal oxyl bonded to Ru in the $Ru(O)Co_3O_4$ cubane is capable of oxidizing chemically inert C−H bonds, motivating further research into cubanes doped by TMs.

Certain iron-based enzymes such as methane monooxygenase[19] and cytochrome P450[20] as well as synthetic catalysts such as Fenton's reagent[21] and iron porphyrins[22] are known to facilitate C−H hydroxylation, which is proposed to proceed through a stepwise oxygen rebound mechanism.[23,24] The first step involves H atom abstraction (HAA) from the organic substrate by the metal-bound oxo ligand, which is followed by

Received: July 31, 2022
Revised: September 4, 2022
Published: September 27, 2022

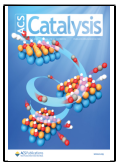

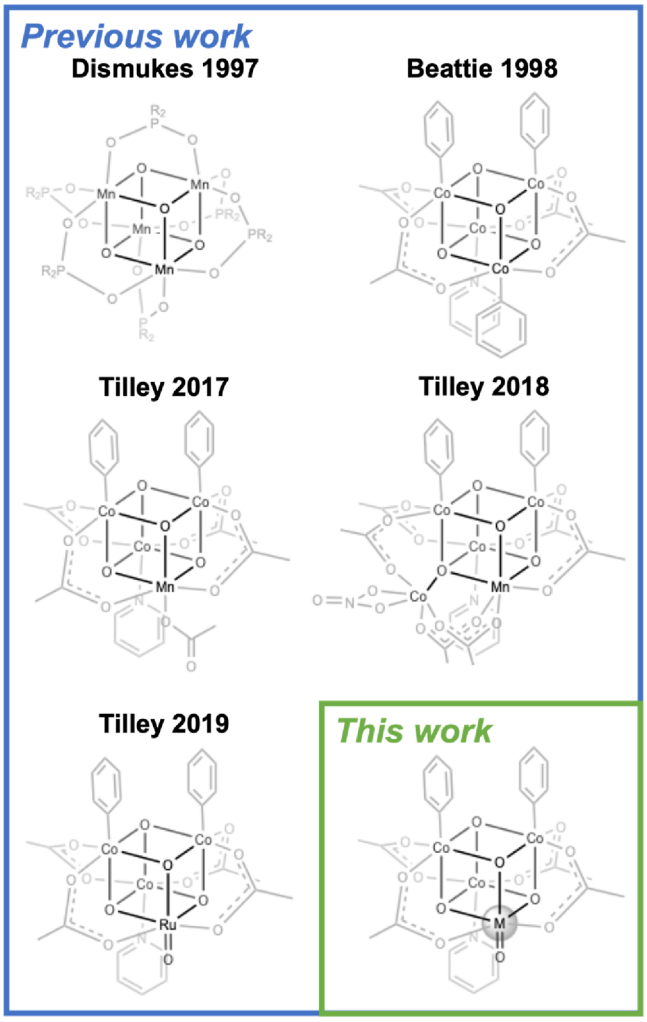

Figure 1. Previously synthesized and studied cubanes along with the cubanes investigated in this work.

the rebound step in which the C−O−H moiety is formed as the hydroxo intermediate reacts with the C-centered radical.[25,26] This mechanism is outlined in Figure 2. In most catalytic systems, the oxo ligand has a radical oxyl character and is generated *in situ* by an oxidant (*e.g.*, hydrogen peroxide).

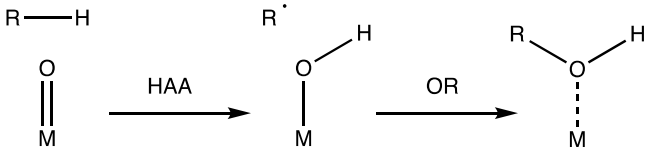

Figure 2. Two-step hydroxylation via the oxygen rebound mechanism. The labels HAA and OR refer to hydrogen atom abstraction and oxygen rebound, respectively.

The oxygen rebound mechanism is now well-established in alkane hydroxylation by heme iron−oxo complexes.[27] However, its precise nature remains a subject of debate due to the exceedingly short lifetime of the radical intermediate,[28] often making the experimental characterization of the rebound step infeasible. In this context, computational chemistry has become a valuable tool to probe the mechanistic nature of metal-catalyzed alkane hydroxylation,[29] attributing the rapidity of the rebound step due to low barriers, which, in some cases, can be smaller than 1 kcal/mol or even nonexistent. Computational studies have also suggested alternative mechanisms for hydroxylation by metal−oxo complexes, including a radical dissociative, nonrebound mechanism that has been verified experimentally.[30]

Nonetheless, a significant limitation of computational studies thus far has been the need to form a hypothesis for the mechanism through which a reaction may proceed prior to computing the desired reaction pathway. Chemical intuition is also essential to successfully locate transition states (TSs) as the outcome of the often-employed saddle point optimization techniques strongly depends on the quality of the initial guess. The necessity of chemical intuition limits the practicality of traditional computational chemistry methods as new reaction mechanisms cannot be discovered unless explicitly considered by the chemist performing the calculations. This highlights the usefulness of recently developed automated reaction mechanism search methods,[31−33] which can discover entirely new chemical reactions and mechanisms, not previously suspected. In particular, the artificial force induced reaction (AFIR) method has proven its reliability when applied to Co-catalyzed hydroformylation,[34] which has been studied thoroughly both experimentally[35] and computationally.[36] Another notable example is the application of AFIR to the three-component Passerini reaction, which revealed that the reaction in fact proceeds via a four-component mechanism.[37]

In this article, we report the spin multiplicity and radical character of a series of $[M(O)Co_3O_4(OAc)_4(py)_3]$ cubanes, where $M(O)$ is a terminal oxo moiety with M = Cr, Mn, Fe, Mo, Tc, Ru, or Rh. Owing to the low cost and low toxicity of iron, we focus on the reactivity of the $[Fe(O)Co_3O_4(OAc)_4(py)_3]$ cubane, which also is found to have a distinct electronic structure within the series. The unusual properties of this cubane are compared to that of the Ru analog focusing on the hydroxylation of methane. Furthermore, the oxygen-rebound nature of the mechanism is verified by means of AFIR calculations.

COMPUTATIONAL DETAILS

All calculations were performed employing spin-unrestricted Kohn−Sham density-functional theory (DFT)[38] as implemented in the Gaussian 16 program package.[39] The hybrid meta-GGA exchange-correlation functional TPSSh[40] was used based on the good agreement between computational geometry optimizations and experimentally observed X-ray crystal structures and between computed and experimental oxidation potentials.[15−18] Geometry optimizations and single-point energy refinement calculations were carried out with the double-ζ def2-SVP and triple-ζ def2-TZVP basis sets,[41] respectively. For numerical integration, we used Gaussian's ultrafine integration grid—that is, a pruned (99,590) grid with 99 radial shells and 590 angular points per shell.

Solvation effects were included by means of the conductor-like polarizable continuum model (C-PCM)[42,43] to implicitly solvate the systems by chloroform or cyclohexane at 298.15 K. Grimme's D3 empirical correction[44] was employed to account for dispersion (with damping coefficients S6 = 1.0, SR6 = 1.223, and S8 = 1.219). Geometry optimizations were carried out without constraints using the Berny algorithm[45] with the geometry optimization energy-represented direct inversion in the iterative subspace method.[46] Intrinsic reaction coordinate (IRC) calculations were performed to verify reactants and products using the Hessian-based predictor−corrector integra-

https://doi.org/10.1021/acscatal.2c03748
ACS Catal. 2022, 12, 12326−12335

tion algorithm.[47,48] Vibrational frequencies were evaluated analytically to verify the minimum nature (for TSs: first order saddle point) of the converged structures. Electron densities were tested for instabilities, which, when found, were relaxed to the ground state. Spin densities were obtained from natural population analyses computed with the NBO6 program.[49] All the manually computed DFT results are available as a dataset collection from the ioChem-BD repository[50] (https://doi.org/10.19061/iochem-bd-6-153).

Automated reaction path searches were performed employing SC-AFIR calculations[33,34,51] using the GRRM20 program[52] with the Gaussian 16 interface for electronic structure calculations (see the Supporting Information for further details on the AFIR calculations). The pure PBE density functional[53] was used together with the def2-SV(P) basis set, including density fitting from the atomic orbital basis. Dispersion was accounted for by Grimme's D3 model (damping coefficients S6 = 1.0, SR6 = 1.217, and S8 = 0.722), and solvation effects of chloroform were included by the C-PCM. The model collision energy parameter γ, which gives an approximate upper bound for the height of barriers traversed in the search, was set to 300 kJ mol^{-1} to ensure that all relevant reaction pathways were investigated. Path refinement calculations, including full TS optimizations, were performed employing the locally updated plane (LUP) method[54,55] as implemented in GRRM20 at the same level of theory as the AFIR calculations but with the larger def2-SVP basis set.

RESULTS AND DISCUSSION

Based on the requirements of having a d^n orbital occupancy with $n > 0$ and being located in front of the oxo wall,[56] which account for catalytic potential and structural stability, respectively, we constructed seven M(O)Co_3O_4 cubanes over the 3d and 4d TM series, with M = Cr, Mn, Fe, Mo, Tc, Ru, and Rh (Figure 1). Only the Ru cubane of this series is known experimentally. The spin state energetics of these cubanes were computed systematically to determine the spin multiplicity of their ground states (*i.e.*, lowest-energy Kohn−Sham determinant; see Tables S1−S7 for details). Table 1 summarizes the results, providing also the local natural spin densities over the terminal oxo ligand (ρ_O) and the metal center to which it is attached (ρ_M).

The spin multiplicity of all oxo cubanes is relatively low, ranging from one to four, which can be rationalized in the context of ligand field theory for the octahedral coordination geometry of the M(O) moiety. Since all metals except Rh have a d-electron count of three or lower, these cubanes are restricted to a spin multiplicity of four or lower, in which only the t_{2g} level is populated. In the case of the Rh cubane, which has a formal 4d^4 configuration, a higher spin multiplicity of five is in principle possible. However, the increased energy gap between the t_{2g} and e_g orbital levels for second-row TMs restricts the electrons to the t_{2g} level, yielding a lower spin multiplicity of three. Furthermore, since the 3d TMs compress the t_{2g} orbitals into a narrower range of energies than the 4d TMs, the former yield cubanes with higher spin multiplicities. The Fe(O)Co_3O_4 and Ru(O)Co_3O_4 cubanes, for instance, share the same d^3 electron count but with a quartet ground state of the Fe cubane and a doublet ground state of the Ru cubane.

Table 1. Computed Ground State Spin Multiplicities (2S + 1) of the M(O)Co_3O_4 Cubanes[a]

M	2S + 1	d^n	ρ_O	ρ_M
Cr	2	d^1	0.19 β	1.05 α
Mn	3	d^2	0.16 β	2.00 α
Fe	4	d^3	0.93 α	1.93 α
Mo	2	d^1	0.07 β	0.87 α
Tc	1	d^2	0.00 α	0.00 α
Ru	2	d^3	0.36 α	0.56 α
Rh	3	d^4	1.11 α	0.75 α

[a]For the M(O) moiety, the formal d electron count (d^n) of the metal is given, together with local natural spin densities of the the oxygen (ρ_O) and metal (ρ_M) in *e*.

As we have shown in a previous work, the reactivity of the terminal M(O) moiety is linearly correlated with ρ_O for [Ru(O)Co_3O_4(OAc)$_4$(4-R-py)$_3$] cubanes (R = OMe, H, CF_3, and Me),[18] implying that this spin density (*i.e.*, the oxyl character, regardless of the spin density at the metal center) can provide a useful measure in the design of C−H activation catalysts based on heterometallic cubanes. Natural bond orbital (NBO) analyses revealed a spin density of ρ_O = 0.36 α in Ru(O)Co_3O_4 (Figure 3) and a significantly larger value of ρ_O = 0.93 α in Fe(O)Co_3O_4 (Figure 3). The oxyl spin density in Ru(O)Co_3O_4 stems from localization of 0.35 unpaired α electrons in the 2p$_y$ orbital, whereas the corresponding spin density at the oxyl in Fe(O)Co_3O_4 is mainly due to 0.48 and 0.38 unpaired α electrons in the 2p$_y$ and 2p$_z$ orbitals, respectively.

Furthermore, the spin density of the metal center, ρ_M, also differs significantly for the two cubanes. Ru(O)Co_3O_4 has a spin density of ρ_{Ru} = 0.56 α with a distinct shape corresponding to the 4d$_{xy}$ orbital, which accounts for 0.48 unpaired α electrons at the metal center. In Fe(O)Co_3O_4, the corresponding spin density at the metal center, ρ_{Fe} = 1.93 α, has a less directional spherical shape, which can be ascribed to the unpaired α electrons being delocalized over the five 3d orbitals (0.44, 0.43, 0.16, 0.32, and 0.56 α electrons in the 3d$_{xy}$, 3d$_{xz}$, 3d$_{yz}$, 3d$_{x2-y2}$, and 3d$_{z2}$ orbitals, respectively). As discussed above, this difference can be related to the tighter energy packing of the Fe 3d orbitals relative to the Ru 4d orbitals, with which the former yields a more delocalized and hybridized spin density at the metal center.

Figure 3 also illustrates the diverse nature of the spin densities across the series. In contrast to the Ru cubane, and in line with the smaller d-electron count, the Cr and Mo cubanes localize most of the spin density over the metal center (1.05 and 0.87 α electrons, respectively). The densities of the Mn and Rh cubanes are similar to that of the Fe cubane, the former being more localized on the metal center (2.00 α electrons) and the latter having a different shape (0.33, 0.21, and 0.13 α electrons in the 4d$_{xy}$, 4d$_{xz}$, and 4d$_{z2}$ orbitals, respectively).

Due to the remarkable oxyl radical character in Fe(O)Co_3O_4 (Figure 3), we investigated the C−H activation reactivity of this cubane in more detail and we compared the results to the reactivity of the related Ru(O)Co_3O_4 cubane. Since several metal complexes with a radical oxyl ligand are known to facilitate the C−H hydroxylation of alkanes,[57,58] we considered the oxidation of cyclohexane to cyclohexanol and the oxidation of methane to methanol by these two cubanes. Although Ru(O)Co_3O_4 and Fe(O)Co_3O_4 may not in fact hydroxylate these two substrates through the oxygen rebound mechanism, the calculation of these mechanisms enables a direct comparison between the reactivity of these two cubanes. The

https://doi.org/10.1021/acscatal.2c03748
ACS Catal. 2022, 12, 12326−12335

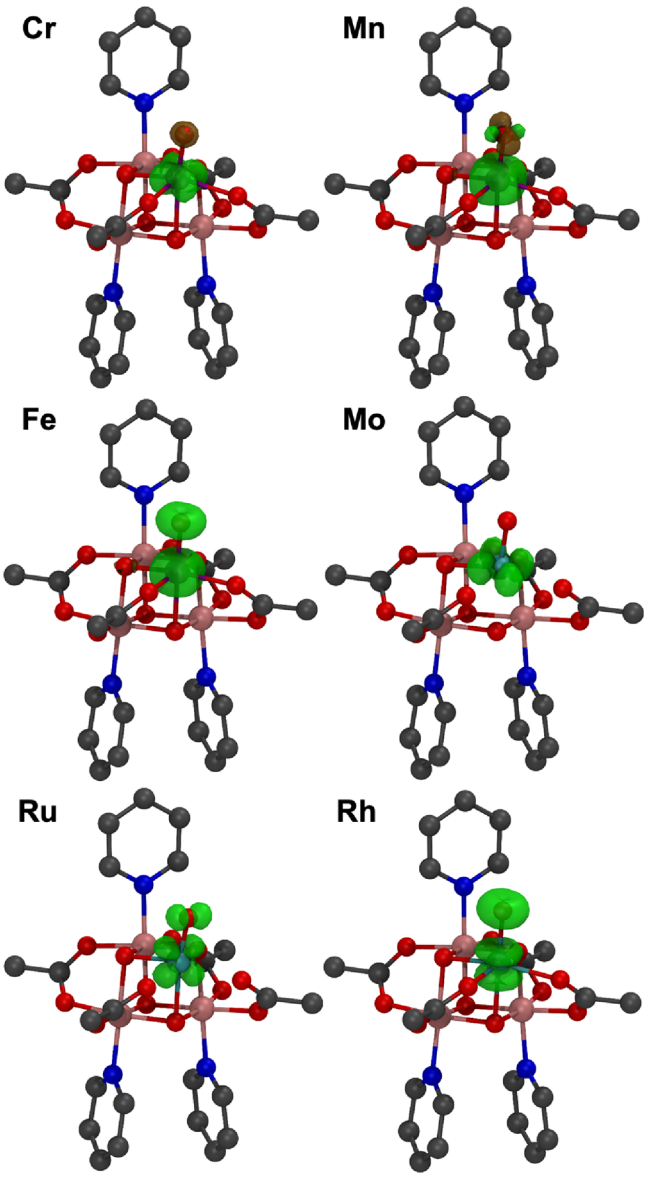

Figure 3. Spin densities over the cubane series (see Table 1 for ρ_O and ρ_M values). An isovalue of 0.02 a.u. was used to plot densities. α and β spin densities appear in green and brown, respectively. All H atoms are omitted for clarity. The Tc cubane was excluded due to the closed-shell nature of its ground state.

rebound pathways were calculated for the ground state multiplicities of the cubanes—that is, quartet (Fe) and doublet (Ru)—along with other spin states of comparable energies to account for possible spin crossover. The results shown in Table 1 also suggest that the Rh cubane, having the largest oxyl character in the series (ρ_O = 1.11 α), can be significantly active in alkane hydroxylation.

The computed reaction profiles for the hydroxylation of cyclohexane by $Ru(O)Co_3O_4$ and $Fe(O)Co_3O_4$ are shown in Figure 4. As the reactant is also used as a solvent, the entropic penalty associated with the first step, $M(O)Co_3O_4 + C_6H_{12} \rightarrow M(O)Co_3O_4\cdots C_6H_{12}$, can be disregarded, effectively lowering the HAA barrier by 3.5 and 5.9 kcal/mol in the case of $Ru(O)Co_3O_4$ and $Fe(O)Co_3O_4$, respectively. Nonetheless, the HAA TS remains 25.7 kcal/mol higher in energy than the $Ru(O)Co_3O_4\cdots C_6H_{12}$ reactant complex. The significant height of this barrier is consistent with the ease of isolating and characterizing the Ru cubane[15,18] despite its oxyl character. The intermediate following the HAA step has a very short lifetime due to the low barrier in the reverse direction (3.8 kcal/mol). The oxygen rebound step could also proceed over an effective barrier of 27.1 kcal/mol (5.2 kcal/mol relative to the intermediate) to yield the $RuCo_3O_4\cdots C_6H_{11}OH$ product, which lies 5.0 kcal/mol below the initial $Ru(O)Co_3O_4\cdots C_6H_{12}$ reactant complex. Subsequent cyclohexanol dissociation is endoergic by 9.8 kcal/mol owing to the vacant site of the resulting $RuCo_3O_4$ complex. Calculations on the quartet state showed that most of the associated reaction pathway is much higher in energy.

Cyclohexane hydroxylation by $Fe(O)Co_3O_4$, on the other hand, is expected to proceed with ease at room temperature since the rate-determining HAA step has an effective barrier of 14.6 kcal/mol upon disregarding the entropic penalty (Figure 4). In contrast to the Ru cubane, in which the energies show potential for spin crossover only in the rebound intermediate, it may happen for Fe during both the HAA and OR steps. In the former step, spin crossover from the quartet to the doublet state reduces the HAA barrier to 13.0 kcal/mol. The rebound barrier is also lower in the doublet state (2.1 kcal/mol) than in the quartet (7.8 kcal/mol), yielding a thermodynamically highly favorable $FeCo_3O_4\cdots C_6H_{11}OH$ complex, from which the cyclohexanol product dissociates in a nearly thermoneutral manner.

The two HAA TSs are structurally equivalent (Figure 5), with M−O−H angles of 112 and 107° for Ru and Fe, respectively, suggesting that the HAA reactivity follows the π reaction channel,[59] with interactions between the ρ_O and σ^*_{C-H} orbitals (Figures S3 and S9). The cleaved C−H bond is elongated in both TSs, by 0.29 and 0.12 Å for $Ru(O)Co_3O_4$ and $Fe(O)Co_3O_4$, respectively. The significantly greater elongation required by the Ru cubane implies lower reactivity, as expected from the weaker radical oxyl character (ρ_O = 0.36 α) relative to Fe cubane (ρ_O = 0.93 α). The oxygen rebound TSs are also similar for the two cubanes, although the orientations of the hydroxyl ligand and cyclohexyl radical differ. The M−O−C angles in the rebound TSs are 123 and 112° for Ru and Fe, respectively, suggesting that the rebound reactivity can also be ascribed to the π channel, with interactions between the p orbitals of the hydroxy ligand and the cyclohexyl radical (Figures S6 and S12). The O···C distances are 2.55 and 2.72 Å for Ru and Fe, respectively, where a longer O···C distance implies that the reaction can proceed more readily, without significant structural distortions, in line with the lower barrier found for Fe. The low height of the OR barriers relative to the HAA is consistent with the radical coupling nature of this reaction, which, in both the Ru and Fe systems, yields a strong C−OH bond.

Based on the cyclohexane hydroxylation results and the terminal oxyl spin density localization rationale, it is expected that $Fe(O)Co_3O_4$ will perform better than $Ru(O)Co_3O_4$ also in the hydroxylation of methane. The computed reaction profiles for this reaction are shown in Figure 6. Due to the very high HAA barrier for $Ru(O)Co_3O_4$ (37.5 kcal/mol), the reaction will not proceed at a reasonable rate under mild conditions. Nonetheless, after traversal of the HAA TS, the reaction should proceed rapidly in either direction, with a barrier of 6.5 kcal/mol in the forward direction and 2.6 kcal/mol in the reverse direction on the doublet spin surface to yield the methanol-coupled product complex or the methane-coupled reactant complex, respectively. Following the rebound

https://doi.org/10.1021/acscatal.2c03748
ACS Catal. 2022, 12, 12326−12335

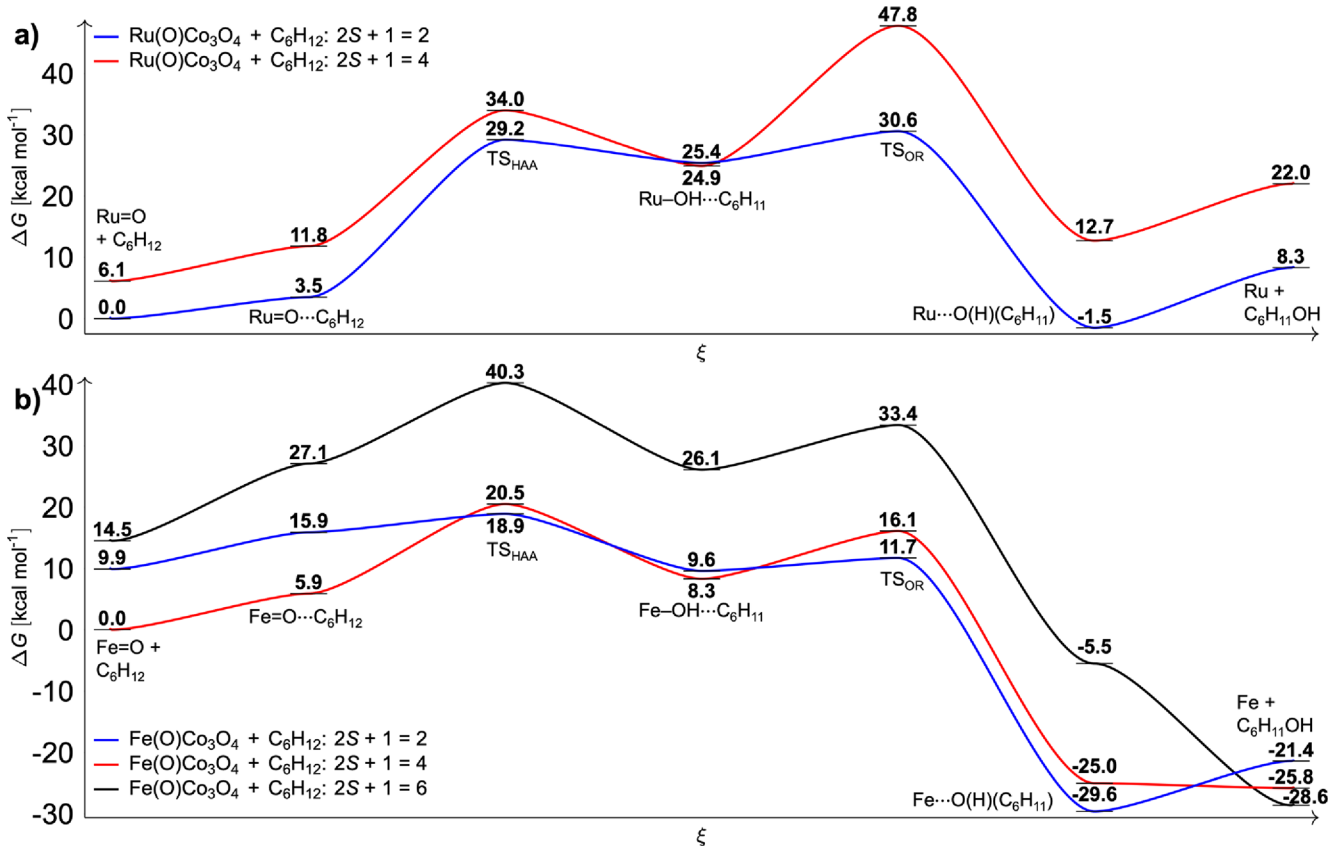

Figure 4. Computed reaction profile for the hydroxylation of cyclohexane by (a) Ru(*O*)Co_3O_4 and (b) Fe(*O*)Co_3O_4, both following the oxygen rebound mechanism. The reaction coordinate, ξ, is given on the *x* axis and the relative free energy, ΔG, is given in kcal/mol on the *y* axis. The TS_{HAA} and TS_{OR} labels refer to the H atom abstraction and oxygen rebound TSs, respectively.

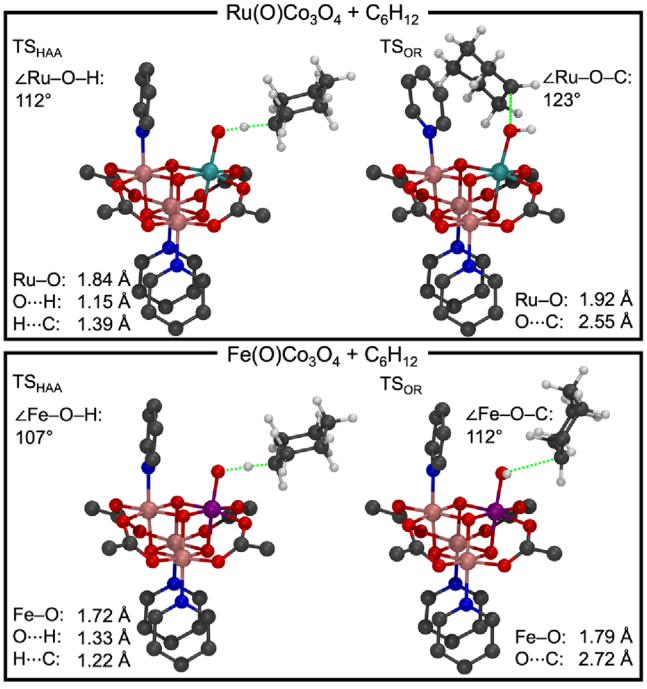

Figure 5. Four TS structures in the hydroxylation of cyclohexane, with the imaginary frequency mode indicated by the dashed green line. All H atoms except those originating from the reactant are omitted for clarity.

reaction step, the $RuCo_3O_4$ cubane is stabilized by coordination to the methanol product, which dissociates with a free energy cost of 6.1 kcal/mol. While the Ru cubane reaction is overall kinetically infeasible, it is also thermodynamically unfavorable, with ΔG = 15.8 kcal/mol. As in the hydroxylation of cyclohexane, spin crossover appears to be irrelevant, with the quartet state being significantly higher in energy for all intermediates except the rebound.

The corresponding Fe-catalyzed hydroxylation is significantly more feasible (Figure 6), with a rate-determining HAA barrier of 24.6 kcal/mol, if the system undergoes a quartet-to-doublet spin crossover similar to that proposed for the cyclohexane reaction (Figure 4). Likewise, the rebound involves a much lower energy barrier (5.3 kcal/mol) and the release of the methanol product in the last step is nearly thermoneutral. Additional spin crossover can happen over the rebound TS region of the potential energy surface, where the double, quartet, and sextet spin surfaces become nearly degenerate. The overall reaction is exergonic, with, for example, ΔG = −13.3 kcal/mol in the doublet state. The moderate energy barrier found for the oxidation of methane, together with the low toxicity and low cost of iron, makes the Fe(*O*)Co_3O_4 cubane a promising catalyst candidate for this reaction. The turnover frequency was calculated according to the energetic span model[60] to be 0.0305 s^{-1} at 373.15 K, which corresponds to a turnover number of 2633 in 24 h. Nonetheless, it should be noted that this significantly high activity might also reduce the stability of the system under the oxidative conditions required for transforming methane into methanol.

https://doi.org/10.1021/acscatal.2c03748
ACS Catal. 2022, 12, 12326−12335

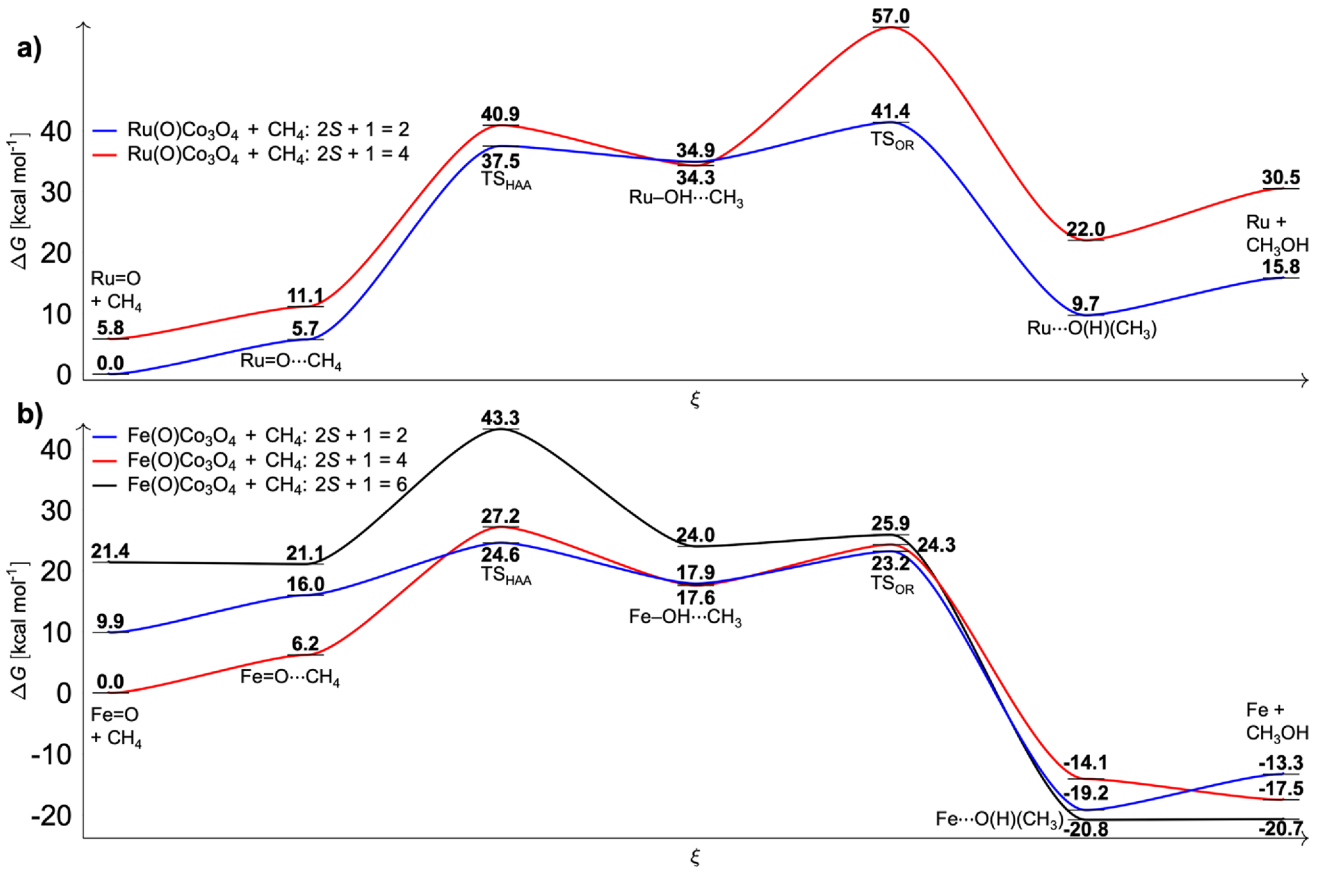

Figure 6. Computed reaction profile for the hydroxylation of CH_4 by (a) Ru(O)Co_3O_4 and (b) Fe(O)Co_3O_4, both following the oxygen rebound mechanism. The reaction coordinate, ξ, is given on the x axis and the relative free energy, ΔG, is given in kcal/mol on the y axis. The TS_{HAA} and TS_{OR} labels refer to the H atom abstraction and oxygen rebound TSs, respectively.

The geometric parameters involved in methane hydroxylation are largely akin to what was observed for cyclohexane, albeit with greater elongation of the cleaved C−H bonds in the HAA TSs and shorter O···C distances in the rebound TS (Figure 7). In the HAA TS, the C−H bond is elongated by 0.36 Å for Ru and 0.20 Å for Fe, becoming significantly longer than in the corresponding cyclohexane activation TSs (by +0.07 and +0.08 Å, respectively). Similarly, the O···C distances in TS_{OR} are 2.33 and 2.48 Å for Ru and Fe, respectively (−0.22 and −0.24 Å shorter than in the cyclohexyl rebound TS). These geometric parameters reflect, like the energetics of the computed reaction pathways, that the hydroxylation of methane is notably more demanding than cyclohexane hydroxylation. The Ru−O−H and Fe−O−H angles of 114 and 111°, and Ru−O−C and Fe−O−C angles of 112 and 109°, in TS_{HAA} and TS_{OR}, respectively, suggest that methane hydroxylation also follows the π channel. Further, the influence of the C−H bond strength on the energy barrier is reflected by the rather large kinetic isotope effect (KIE) k_H/k_D = 9.59 that was computed for the rate-determining HAA step of the Fe-catalyzed methane hydroxylation.

The computed oxygen rebound mechanism is likely to be the mechanism through which the cubanes and the organic substrates react. Nonetheless, manual DFT calculations performed based on chemical intuition cannot avoid the pitfall of human errors such as overlooking chemically relevant reaction pathways. Automated reaction mechanism discovery methods provide a reliable approach to probe whether the computed reaction pathway is indeed the most favorable. To address this, we performed two separate AFIR calculations for the reaction between Fe(O)Co_3O_4 and CH_4 in the doublet state.

The first AFIR calculation explored intermediates seemingly accessible via a single TS starting from the initial Fe(O)-Co_3O_4···CH4 reactant complex (Figure 8a), whereas the second AFIR calculation explored intermediates accessible via a single TS starting from the Fe(OH)Co_3O_4···CH_3 intermediate obtained in the first AFIR calculation (Figure 8b). Figure 8 shows that the thermodynamically most favorable product is indeed the $FeCo_3O_4$···CH_3OH product complex (**EQ9** in Figure 8b), in agreement with the manually computed reaction profile (Figure 6b). As shown by both the manual DFT calculations and the AFIR calculations, the methanol-coupled product complex is kinetically accessible through the oxygen rebound mechanism (**EQ0** → **EQ1**, **EQ1** → **EQ9** in Figure 8).

The first AFIR calculation (Figure 8a) shows that the reactant complex (**EQ0**) may transform into seven other intermediates (**EQ1**−**EQ7**), presumably via a single TS, though some of these intermediates are equivalent in terms of molecular connectivity—in particular, **EQ2**, **EQ3**, and **EQ5** are all equivalent to **EQ0**, while **EQ6** and **EQ7** are equivalent to each other. The energy differences within these two groups of geometries are small and can be ascribed to minor conformational rearrangements. This yields a total of four intermediates with distinct connectivity, represented by **EQ0**, **EQ1**, **EQ4**, and **EQ6**. Among these, **EQ0** is the initial Fe(O)Co_3O_4···CH_4 reactant complex, however since **EQ5** is

https://doi.org/10.1021/acscatal.2c03748
ACS Catal. 2022, 12, 12326−12335

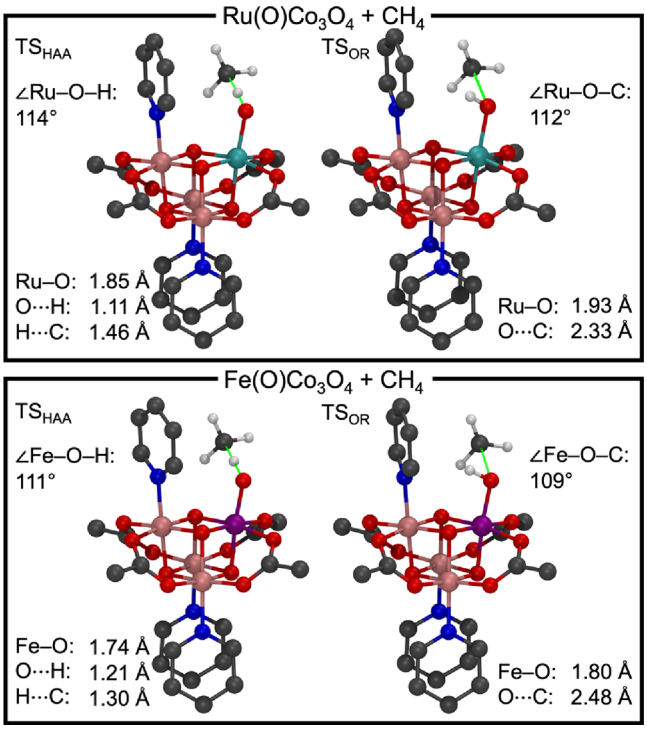

Figure 7. Four TS structures in the hydroxylation of methane, with the imaginary frequency mode indicated by the dashed green line. All H atoms except those originating from the reactant are omitted for clarity.

the lowest-energy reactant species, **EQ5** is used as the energy reference rather than **EQ0**. **EQ1** is the Fe(*OH*)Co_3O_4···CH_3 intermediate complex resulting from HAA, while **EQ4** is the product resulting from hydroxylation and subsequent methanol dissociation from the cubane. At last, **EQ7** is a structure similar to the initial reactant complex, although less stable than **EQ5** by 10.6 kcal/mol, in which one acetate ligand has undergone partial decoordination from κ^2 to κ^1, with the dangling O making a H-bond to methane.

In the second AFIR calculation (Figure 8b), eight intermediates (**EQ8**–**EQ15**) were obtained starting from **EQ1**, which can be separated into five distinct intermediates. **EQ8** corresponds to an Fe(OH)(CH_3)Co_3O_4 hydroxy–methyl complex in which the $CH_3^{\bullet}$ radical is bonded to the metal center. This is a rather exotic and unexpected intermediate in a rebound pathway, which can also be regarded as the product of the oxidative addition of the methanol product to the reduced form of the cubane. However, it has a high relative energy of 34.0 kcal/mol, making it irrelevant to the overall reaction. In contrast, **EQ12** is a stable complex (3.1 kcal/mol above **EQ5**), which contains the Fe(OH) moiety, where the methyl radical is coupled with a bridging oxo ligand. The single κ^1-acetate ligand of **EQ12** is also present in **EQ7**, and these two intermediates together can be seen as part of an alternative pathway, competing with the rebound mechanism, in which the methyl radical is trapped by the cubane core. **EQ9**, **EQ10**, and **EQ13** are different conformers of the methanol-coordinated $FeCo_3O_4$···CH_3OH product complex, which is the thermodynamically most stable intermediate, whereas **EQ11** corresponds to the initial Fe(*O*)Co_3O_4···CH_4 reactant complex (**EQ0**). **EQ14** would

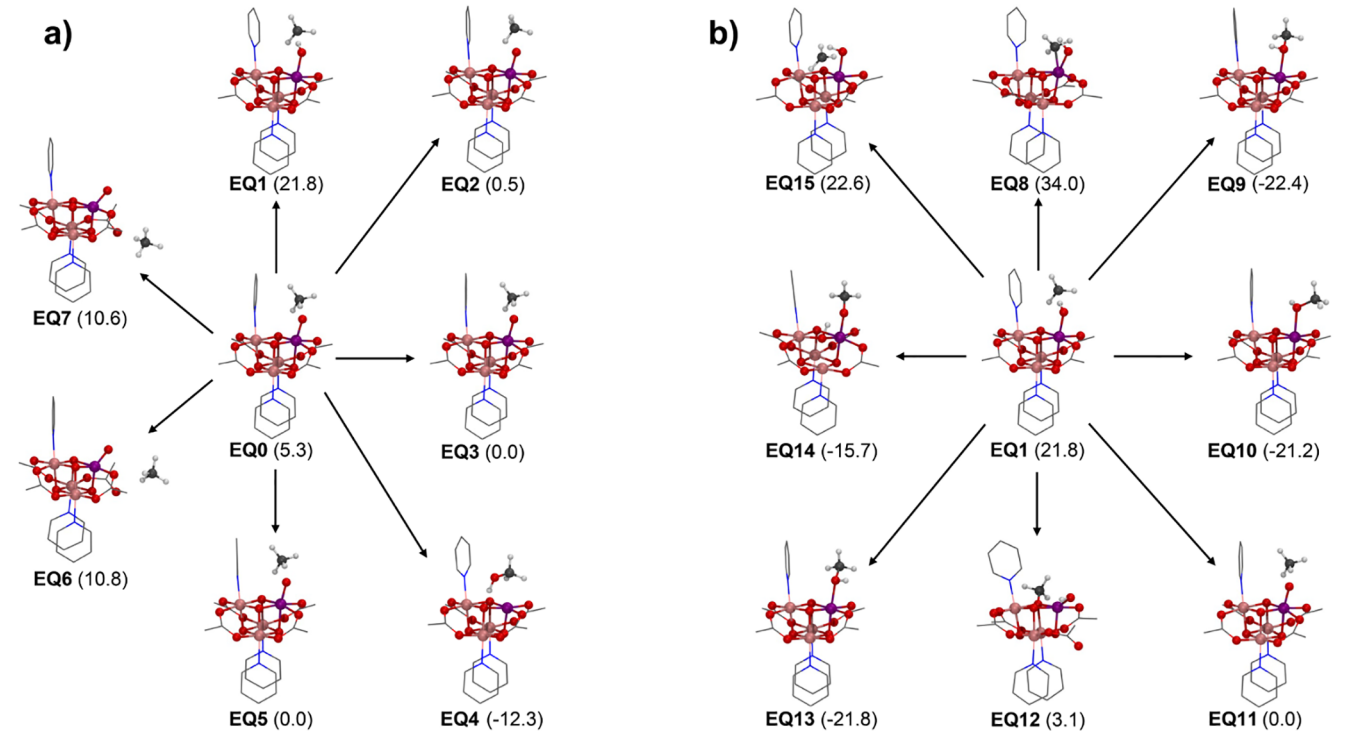

Figure 8. Intermediates obtained by the two AFIR calculations starting from the (a) initial Fe(*O*)Co_3O_4···CH_4 reactant complex (**EQ0**) and the (b) Fe(*OH*)Co_3O_4···CH_3 intermediate obtained in the first AFIR calculation (**EQ1**). Relative energies, ΔE, are given in parantheses in units of kcal/mol relative to the lowest-energy reactant species (**EQ5**). All H atoms except those originating from the methane reactant are omitted for clarity. The line representation is used for the pyridine and acetate ligands only for the sake of clarity. The same DFT (PBE/def2-SV(P)) level of theory was used for the entire system. All calculations were carried out in the doublet state.

https://doi.org/10.1021/acscatal.2c03748
ACS Catal. 2022, 12, 12326−12335

result from an endothermic intramolecular proton transfer in the **EQ9** product. Finally, **EQ15** is structurally equivalent to **EQ1**, but with a slightly different orientation of the methyl radical.

It is worth noting that exact TSs were not located in the initial AFIR path searches because of the high computational cost. The combination of the artificial force applied to the potential energy landscape and the shallow nature of the potential energy well in which the Fe−OH···CH_3 intermediate is located resulted in the first AFIR calculation incorrectly, indicating that the hydroxylation may proceed via a single TS[61] (**EQ0** → **EQ4** in Figure 8a). Upon refining the pathway in question, including exact TS optimization, it became evident that the reaction cannot take place in a single step. Instead, the reaction pathway consists of three steps, including the two-step oxygen rebound mechanism followed by methanol dissociation. The refined minimum energy paths (Figures S33−35) were generated in an automated manner, including IRC calculations. Further, these paths were equivalent to the manually computed doublet reaction pathway of Figure 6b and the pathway found by the AFIR calculations (**EQ0** → **EQ1** → **EQ9**; see the SI for further details).

CONCLUSIONS

In this work, we presented a detailed and systematic investigation of the electronic structure and reactivity of $M(O)Co_3O_4$ cubanes possessing a terminal oxo ligand. We provided a rationale for the computed ground state spin multiplicities of the cubanes and demonstrated how the spin multiplicity relates to reactivity through the localization of the spin density on the terminal oxo, yielding an oxyl ligand. The catalytic properties of the $Fe(O)Co_3O_4$ cubane were probed by means of DFT calculations for the hydroxylation of cyclohexane and methane and compared to those of the $Ru(O)Co_3O_4$ cubane. The Fe-based cubane displays enhanced C−H activation performance due to the increased oxyl radical character relative to $Ru(O)Co_3O_4$.

We also demonstrated the potential of automated reaction mechanism discovery methods, by means of AFIR calculations, to uncover relevant reaction pathways essential in the computational design of organometallic catalysts. These calculations showed that the oxygen rebound mechanism yields the lowest-energy pathway for methane hydroxylation by $Fe(O)Co_3O_4$. Remarkably, AFIR revealed two additional intermediates outside the traditional pathway, in which the methyl does not undergo the rebound of the OH ligand but rather couples with either the metal center or a bridging oxo.

Based on these results, we propose the $Fe(O)Co_3O_4$ cubane as a potential methane hydroxylation catalyst. Furthermore, the insights of this study may be generalized to enable the design of novel C−H hydroxylation catalysts bearing a terminal oxyl ligand that promote the oxidation of this and other substrates. A design strategy can be to enhance the radical oxyl character, which may be accomplished by replacing Co atoms from the cubane core by other late 3d TM metals stabilizing high-spin states. Nevertheless, a very high radical character at the terminal oxyl may render the complex too unstable and thus either not synthesizable[52,62] or not robust for catalysis. It is necessary to find the optimal balance between reactivity and stability, which remains an intricate challenge involving both the metal core and the supporting ligands.

ASSOCIATED CONTENT

Supporting Information

The Supporting Information is available free of charge at https://pubs.acs.org/doi/10.1021/acscatal.2c03748.

Optimized geometries and energies of all stationary points, further details on the AFIR calculations, and a comparison between the TPSSh and PBE levels of theory (PDF)

AUTHOR INFORMATION

Corresponding Author

David Balcells − *Hylleraas Centre for Quantum Molecular Sciences, Department of Chemistry, University of Oslo, 0315 Oslo, Norway;* orcid.org/0000-0002-3389-0543; Email: david.balcells@kjemi.uio.no

Authors

Bastian Bjerkem Skjelstad − *Hylleraas Centre for Quantum Molecular Sciences, Department of Chemistry, University of Oslo, 0315 Oslo, Norway; Graduate School of Chemical Sciences and Engineering, Hokkaido University, Sapporo 060-8628, Japan;* orcid.org/0000-0002-9769-6459

Trygve Helgaker − *Hylleraas Centre for Quantum Molecular Sciences, Department of Chemistry, University of Oslo, 0315 Oslo, Norway*

Satoshi Maeda − *Department of Chemistry, Faculty of Science, Hokkaido University, Sapporo 060-0810, Japan; Institute for Chemical Reaction Design and Discovery (WPI-ICReDD), Hokkaido University, Sapporo 001-0021, Japan;* orcid.org/0000-0001-8822-1147

Complete contact information is available at: https://pubs.acs.org/10.1021/acscatal.2c03748

Notes

The authors declare no competing financial interest.

ACKNOWLEDGMENTS

B.B.S., T.H., and D.B. acknowledge the support from the Research Council of Norway through its Centers of Excellence scheme (Hylleraas Centre for Quantum Molecular Sciences; project 262695) and the Norwegian Metacenter for Computational Science (NOTUR; project nn4654k). B.B.S. is supported by a scholarship from the Otsuka Toshimi Scholarship Foundation and a grant from the Japan Science and Technology Agency (JST) under the Support for Pioneering Research Initiated by the Next Generation (SPRING) program (grant number JPMJSP2119). We thank Prof. T. Don Tilley for helpful conversations.

REFERENCES

(1) Amtawong, J.; Nguyen, A. I.; Tilley, T. D. Mechanistic Aspects of Cobalt−Oxo Cubane Clusters in Oxidation Chemistry. *J. Am. Chem. Soc.* **2022**, *144*, 1475−1492.

(2) Kawakami, K.; Umena, Y.; Kamiya, N.; Shen, J.-R. Structure of the Catalytic, Inorganic Core of Oxygen-Evolving Photosystem II at 1. 9Å Resolution. *J. Photochem. Photobiol., B* **2011**, *104*, 9−18.

(3) Suga, M.; Akita, F.; Hirata, K.; Ueno, G.; Murakami, H.; Nakajima, Y.; Shimizu, T.; Yamashita, K.; Yamamoto, M.; Ago, H.; Shen, J.-R. Native Structure of Photosystem II at 1. 95 Å Resolution Viewed by Femtosecond X-Ray Pulses. *Nature* **2015**, *517*, 99−103.

(4) Kok, B.; Forbush, B.; McGloin, M. Cooperation of Charges in Photosynthetic O $_2$ Evolution−I. A Linear Four Step Mechanism. *Photochem. Photobiol.* **1970**, *11*, 457−475.

(5) Haumann, M.; Liebisch, P.; Müller, C.; Barra, M.; Grabolle, M.; Dau, H. Photosynthetic O_2 Formation Tracked by Time-Resolved X-Ray Experiments. *Science* **2005**, *310*, 1019−1021.
(6) McEvoy, J. P.; Brudvig, G. W. Water-Splitting Chemistry of Photosystem II. *Chem. Rev.* **2006**, *106*, 4455−4483.
(7) Ruettinger, W. F.; Campana, C.; Dismukes, G. C. Synthesis and Characterization of $Mn_4O_4L_6$ Complexes with Cubane-like Core Structure: A New Class of Models of the Active Site of the Photosynthetic Water Oxidase. *J. Am. Chem. Soc.* **1997**, *119*, 6670−6671.
(8) Yagi, M.; Wolf, K. V.; Baesjou, P. J.; Bernasek, S. L.; Dismukes, G. C. Selective Photoproduction of O2 from the Mn4O4 Cubane Core: A Structural and Functional Model for the Photosynthetic Water-Oxidizing Complex. *Angew. Chem., Int. Ed.* **2001**, *40*, 2925−2928.
(9) Dismukes, G. C.; Brimblecombe, R.; Felton, G. A. N.; Pryadun, R. S.; Sheats, J. E.; Spiccia, L.; Swiegers, G. F. Development of Bioinspired Mn_4O_4−Cubane Water Oxidation Catalysts: Lessons from Photosynthesis. *Acc. Chem. Res.* **2009**, *42*, 1935−1943.
(10) Beattie, J. K.; Hambley, T. W.; Klepetko, J. A.; Masters, A. F.; Turner, P. The Chemistry of Cobalt Acetate—IV. The Isolation and Crystal Structure of the Symmetric Cubane, Tetrakis[(μ-Acetato)-(M3-Oxo) (Pyridine)Cobalt(III)] · Chloroform Solvate, [Co4(M3-O)4(μ-CH3CO2)4(C5H5N)In4] · 5CHCl3 and of the Dicationic Partial Cubane, Trimeric, [(μ-Acetato)(Acetato)Tris(μ-Hdyroxy-(M3-Oxo) Hexakispyridinetricobalt(III)]Hexafluorophosphate · Water Solvate, [Co3(M3-O)(μ-OH)3(μ-CH3CO2)CH3CO2-(C5H5N)6)PF6]2 · 2H2O. *Polyhedron* **1998**, *17*, 1343−1354.
(11) Kanan, M. W.; Nocera, D. G. In Situ Formation of an Oxygen-Evolving Catalyst in Neutral Water Containing Phosphate and Co^{2+}. *Science* **2008**, *321*, 1072−1075.
(12) McCool, N. S.; Robinson, D. M.; Sheats, J. E.; Dismukes, G. C. A Co_4O_4 "Cubane" Water Oxidation Catalyst Inspired by Photosynthesis. *J. Am. Chem. Soc.* **2011**, *133*, 11446−11449.
(13) Nguyen, A. I.; Van Allsburg, K. M.; Terban, M. W.; Bajdich, M.; Oktawiec, J.; Amtawong, J.; Ziegler, M. S.; Dombrowski, J. P.; Lakshmi, K. V.; Drisdell, W. S.; Yano, J.; Billinge, S. J. L.; Tilley, T. D. Stabilization of Reactive Co_4O_4 Cubane Oxygen-Evolution Catalysts within Porous Frameworks. *Proc. Natl. Acad. Sci. U. S. A.* **2019**, 201815013.
(14) Nguyen, A. I.; Suess, D. L. M.; Darago, L. E.; Oyala, P. H.; Levine, D. S.; Ziegler, M. S.; Britt, R. D.; Tilley, T. D. Manganese−Cobalt Oxido Cubanes Relevant to Manganese-Doped Water Oxidation Catalysts. *J. Am. Chem. Soc.* **2017**, *139*, 5579−5587.
(15) Amtawong, J.; Balcells, D.; Wilcoxen, J.; Handford, R. C.; Biggins, N.; Nguyen, A. I.; Britt, R. D.; Tilley, T. D. Isolation and Study of Ruthenium−Cobalt Oxo Cubanes Bearing a High-Valent, Terminal Ru^{V}−Oxo with Significant Oxyl Radical Character. *J. Am. Chem. Soc.* **2019**, *141*, 19859−19869.
(16) Nguyen, A. I.; Darago, L. E.; Balcells, D.; Tilley, T. D. Influence of a "Dangling" Co(II) Ion Bound to a $[MnCo_3O_4]$ Oxo Cubane. *J. Am. Chem. Soc.* **2018**, *140*, 9030−9033.
(17) Amtawong, J.; Skjelstad, B. B.; Balcells, D.; Tilley, T. D. Concerted Proton−Electron Transfer Reactivity at a Multimetallic Co_4O_4 Cubane Cluster. *Inorg. Chem.* **2020**, *59*, 15553−15560.
(18) Amtawong, J.; Skjelstad, B. B.; Handford, R. C.; Suslick, B. A.; Balcells, D.; Tilley, T. D. C−H Activation by $RuCo_3O_4$ Oxo Cubanes: Effects of Oxyl Radical Character and Metal−Metal Cooperativity. *J. Am. Chem. Soc.* **2021**, *143*, 12108−12119.
(19) Tinberg, C. E.; Lippard, S. J. Dioxygen Activation in Soluble Methane Monooxygenase. *Acc. Chem. Res.* **2011**, *44*, 280−288.
(20) Meunier, B.; de Visser, S. P.; Shaik, S. Mechanism of Oxidation Reactions Catalyzed by Cytochrome P450 Enzymes. *Chem. Rev.* **2004**, *104*, 3947−3980.
(21) Ensing, B.; Buda, F.; Gribnau, M. C. M.; Baerends, E. J. Methane-to-Methanol Oxidation by the Hydrated Iron(IV) Oxo Species in Aqueous Solution: A Combined DFT and Car−Parrinello Molecular Dynamics Study. *J. Am. Chem. Soc.* **2004**, *126*, 4355−4365.
(22) Filatov, M.; Harris, N.; Shaik, S. On the "Rebound" Mechanism of Alkane Hydroxylation by Cytochrome P450: Electronic Structure of the Intermediate and the Electron Transfer Character in the Rebound Step. *Angew. Chem., Int. Ed.* **1999**, *38*, 3510−3512.
(23) Groves, J. T. Key Elements of the Chemistry of Cytochrome P-450: The Oxygen Rebound Mechanism. *J. Chem. Educ.* **1985**, *62*, 928.
(24) (a) Huang, X.; Groves, J. T. Beyond Ferryl-Mediated Hydroxylation: 40 Years of the Rebound Mechanism and C−H Activation. *J. Biol. Inorg. Chem.* **2017**, *22*, 185−207. (b) Rana, S.; Biswas, J. P.; Paul, S.; Paik, A.; Maiti, D. Organic synthesis with the most abundant transition metal−iron: from rust to multitasking catalysts. *Chem. Soc. Rev.* **2021**, *50*, 243−472. (c) Sameera, W. M. C.; McGrady, J. E. *Dalton Trans.* **2008**, 6141−6149.
(25) Balcells, D.; Clot, E.; Eisenstein, O. C—H Bond Activation in Transition Metal Species from a Computational Perspective. *Chem. Rev.* **2010**, *110*, 749−823.
(26) Balcells, D.; Eisenstein, O. Theoretical Studies on the Reaction Mechanism of Metal-Assisted CH Activation. In *Comprehensive Inorganic Chemistry II*; Elsevier, 2013; pp. 695−726.
(27) Cho, K.-B.; Hirao, H.; Shaik, S.; Nam, W. To Rebound or Dissociate? This Is the Mechanistic Question in C−H Hydroxylation by Heme and Nonheme Metal−Oxo Complexes. *Chem. Soc. Rev.* **2016**, *45*, 1197−1210.
(28) Shaik, S.; Cohen, S.; de Visser, S. P.; Sharma, P. K.; Kumar, D.; Kozuch, S.; Ogliaro, F.; Danovich, D. The "Rebound Controversy:" An Overview and Theoretical Modeling of the Rebound Step in C−H Hydroxylation by Cytochrome P450. *Eur. J. Inorg. Chem.* **2004**, *2004*, 207−226.
(29) Shaik, S.; Cohen, S.; Wang, Y.; Chen, H.; Kumar, D.; Thiel, W. P450 Enzymes: Their Structure, Reactivity, and Selectivity—Modeled by QM/MM Calculations. *Chem. Rev.* **2010**, *110*, 949−1017.
(30) Cho, K.-B.; Wu, X.; Lee, Y.-M.; Kwon, Y. H.; Shaik, S.; Nam, W. Evidence for an Alternative to the Oxygen Rebound Mechanism in C−H Bond Activation by Non-Heme $Fe^{IV}O$ Complexes. *J. Am. Chem. Soc.* **2012**, *134*, 20222−20225.
(31) Dewyer, A. L.; Argüelles, A. J.; Zimmerman, P. M. Methods for Exploring Reaction Space in Molecular Systems. *WIREs Comput. Mol. Sci.* **2018**, *8*, No. e1354.
(32) Simm, G. N.; Vaucher, A. C.; Reiher, M. Exploration of Reaction Pathways and Chemical Transformation Networks. *J. Phys. Chem. A* **2019**, *123*, 385−399.
(33) Maeda, S.; Harabuchi, Y. Exploring Paths of Chemical Transformations in Molecular and Periodic Systems: An Approach Utilizing Force. *WIREs Comput. Mol. Sci.* **2021**, *11*, No. e1538.
(34) Maeda, S.; Harabuchi, Y.; Takagi, M.; Taketsugu, T.; Morokuma, K. Artificial Force Induced Reaction (AFIR) Method for Exploring Quantum Chemical Potential Energy Surfaces. *Chem. Rec.* **2016**, *16*, 2232−2248.
(35) Hebrard, F.; Kalck, P. Cobalt-Catalyzed Hydroformylation of Alkenes: Generation and Recycling of the Carbonyl Species, and Catalytic Cycle. *Chem. Rev.* **2009**, *109*, 4272−4282.
(36) Rush, L. E.; Pringle, P. G.; Harvey, J. N. Computational Kinetics of Cobalt-Catalyzed Alkene Hydroformylation. *Angew. Chem., Int. Ed.* **2014**, *53*, 8672−8676.
(37) Maeda, S.; Komagawa, S.; Uchiyama, M.; Morokuma, K. Finding Reaction Pathways for Multicomponent Reactions: The Passerini Reaction Is a Four-Component Reaction. *Angew. Chem., Int. Ed.* **2011**, *50*, 644−649.
(38) Kohn, W.; Sham, L. J. Self-Consistent Equations Including Exchange and Correlation Effects. *Phys. Rev.* **1965**, *140*, A1133−A1138.
(39) Frisch, M. J.; Trucks, G. W.; Schlegel, H. B.; Scuseria, G. E.; Robb, M. A.; Cheeseman, J. R.; Scalmani, G.; Barone, V.; Petersson, G. A.; Nakatsuji, H.; Li, X.; Caricato, M.; Marenich, A. V.; Bloino, J.; Janesko, B. G.; Gomperts, R.; Mennucci, B.; Hratchian, H. P.; Ortiz, J. V.; Izmaylov, A. F.; Sonnenberg, J. L.; Williams-Young, D.; Ding, F.; Lipparini, F.; Egidi, F.; Goings, J.; Peng, B.; Petrone, A.; Henderson, T.; Ranasinghe, D.; Zakrzewski, V. G.; Gao, J.; Rega, N.; Zheng, G.; Liang, W.; Hada, M.; Ehara, M.; Toyota, K.; Fukuda, R.; Hasegawa, J.;

https://doi.org/10.1021/acscatal.2c03748
ACS Catal. 2022, 12, 12326−12335

Ishida, M.; Nakajima, T.; Honda, Y.; Kitao, O.; Nakai, H.; Vreven, T.; Throssell, K.; Montgomery, J. A., Jr.; Peralta, J. E.; Ogliaro, F.; Bearpark, M. J.; Heyd, J. J.; Brothers, E. N.; Kudin, K. N.; Staroverov, V. N.; Keith, T. A.; Kobayashi, R.; Normand, J.; Raghavachari, K.; Rendell, A. P.; Burant, J. C.; Iyengar, S. S.; Tomasi, J.; Cossi, M.; Millam, J. M.; Klene, M.; Adamo, C.; Cammi, R.; Ochterski, J. W.; Martin, R. L.; Morokuma, K.; Farkas, O.; Foresman, J. B.; Fox, D. J. *Gaussian~16* Revision C.01, 2016.

(40) Staroverov, V. N.; Scuseria, G. E.; Tao, J.; Perdew, J. P. Comparative Assessment of a New Nonempirical Density Functional: Molecules and Hydrogen-Bonded Complexes. *J. Chem. Phys.* **2003**, *119*, 12129−12137.

(41) Weigend, F.; Ahlrichs, R. Balanced Basis Sets of Split Valence, Triple Zeta Valence and Quadruple Zeta Valence Quality for H to Rn: Design and Assessment of Accuracy. *Phys. Chem. Chem. Phys.* **2005**, *7*, 3297.

(42) Barone, V.; Cossi, M. Quantum Calculation of Molecular Energies and Energy Gradients in Solution by a Conductor Solvent Model. *J. Phys. Chem. A* **1998**, *102*, 1995−2001.

(43) Cossi, M.; Rega, N.; Scalmani, G.; Barone, V. Energies, Structures, and Electronic Properties of Molecules in Solution with the C-PCM Solvation Model. *J. Comput. Chem.* **2003**, *24*, 669−681.

(44) Grimme, S.; Antony, J.; Ehrlich, S.; Krieg, H. A Consistent and Accurate *Ab Initio* Parametrization of Density Functional Dispersion Correction (DFT-D) for the 94 Elements H-Pu. *J. Chem. Phys.* **2010**, *132*, 154104.

(45) Simons, J.; Joergensen, P.; Taylor, H.; Ozment, J. Walking on Potential Energy Surfaces. *J. Phys. Chem.* **1983**, *87*, 2745−2753.

(46) Li, X.; Frisch, M. J. Energy-Represented Direct Inversion in the Iterative Subspace within a Hybrid Geometry Optimization Method. *J. Chem. Theory Comput.* **2006**, *2*, 835−839.

(47) Hratchian, H. P.; Schlegel, H. B. Accurate Reaction Paths Using a Hessian Based Predictor−Corrector Integrator. *J. Chem. Phys.* **2004**, *120*, 9918−9924.

(48) Hratchian, H. P.; Schlegel, H. B. Using Hessian Updating To Increase the Efficiency of a Hessian Based Predictor-Corrector Reaction Path Following Method. *J. Chem. Theory Comput.* **2005**, *1*, 61−69.

(49) Glendening, E. D.; Landis, C. R.; Weinhold, F. *NBO 6.0* : Natural Bond Orbital Analysis Program. *J. Comput. Chem.* **2013**, *34*, 1429−1437.

(50) Álvarez-Moreno, M.; de Graaf, C.; López, N.; Maseras, F.; Poblet, J. M.; Bo, C. Managing the Computational Chemistry Big Data Problem: The **IoChem-BD** Platform. *J. Chem. Inf. Model.* **2015**, *55*, 95−103.

(51) Maeda, S.; Harabuchi, Y.; Takagi, M.; Saita, K.; Suzuki, K.; Ichino, T.; Sumiya, Y.; Sugiyama, K.; Ono, Y. Implementation and Performance of the Artificial Force Induced Reaction Method in the GRRM17 Program. *J. Comput. Chem.* **2018**, *39*, 233−251.

(52) Maeda, S.; Ohno, K.; Morokuma, K. Systematic Exploration of the Mechanism of Chemical Reactions: The Global Reaction Route Mapping (GRRM) Strategy Using the ADDF and AFIR Methods. *Phys. Chem. Chem. Phys.* **2013**, *15*, 3683.

(53) Perdew, J. P.; Burke, K.; Ernzerhof, M. Generalized Gradient Approximation Made Simple. *Phys. Rev. Lett.* **1996**, *77*, 3865−3868.

(54) Choi, C.; Elber, R. Reaction Path Study of Helix Formation in Tetrapeptides: Effect of Side Chains. *J. Chem. Phys.* **1991**, *94*, 751−760.

(55) Ayala, P. Y.; Schlegel, H. B. A Combined Method for Determining Reaction Paths, Minima, and Transition State Geometries. *J. Chem. Phys.* **1997**, *107*, 375−384.

(56) Winkler, J. R.; Gray, H. B. Electronic Structures of Oxo-Metal Ions. In *Molecular Electronic Structures of Transition Metal Complexes I*; Mingos, D. M. P.; Day, P.; Dahl, J. P., Eds.; Structure and Bonding; Springer Berlin Heidelberg: Berlin, Heidelberg, 2011; Vol. *142*, pp. 17−28.

(57) Feyel, S.; Döbler, J.; Schröder, D.; Sauer, J.; Schwarz, H. Thermal Activation of Methane by Tetranuclear [V4O10]+. *Angew. Chem., Int. Ed.* **2006**, *45*, 4681−4685.

(58) Zhang, X.; Schwarz, H. Thermal Activation of Methane by Diatomic Metal Oxide Radical Cations: PbO+· as One of the Missing Pieces. *ChemCatChem* **2010**, *2*, 1391−1394.

(59) Ye, S.; Geng, C.-Y.; Shaik, S.; Neese, F. Electronic Structure Analysis of Multistate Reactivity in Transition Metal Catalyzed Reactions: The Case of C−H Bond Activation by Non-Heme Iron(Iv)−Oxo Cores. *Phys. Chem. Chem. Phys.* **2013**, *15*, 8017.

(60) Kozuch, S.; Shaik, S. How to Conceptualize Catalytic Cycles? The Energetic Span Model. *Acc. Chem. Res.* **2011**, *44*, 101−110.

(61) Zhou, M.; Balcells, D.; Parent, A. R.; Crabtree, R. H.; Eisenstein, O. Cp* Iridium Precatalysts for Selective C−H Oxidation via Direct Oxygen Insertion: A Joint Experimental/Computational Study. *ACS Catal.* **2012**, *2*, 208−218.

(62) Sumiya, Y.; Harabuchi, Y.; Nagata, Y.; Maeda, S. Quantum Chemical Calculations to Trace Back Reaction Paths for the Prediction of Reactants. *JACS Au* **2022**, *2*, 1181−1188.

https://doi.org/10.1021/acscatal.2c03748
ACS Catal. 2022, 12, 12326−12335